CBGL: Fast Monte Carlo Passive Global Localisation of 2D LIDAR Sensor

Alexandros Filotheou

Abstract— Navigation of a mobile robot is conditioned on the knowledge of its pose. In observer-based localisation configurations its initial pose may not be knowable in advance, leading to the need of its estimation. Solutions to the problem of global localisation are either robust against noise and environment arbitrariness but require motion and time, which may (need to) be economised on, or require minimal estimation time but assume environmental structure, may be sensitive to noise, and demand preprocessing and tuning. This article proposes a method that retains the strengths and avoids the weaknesses of the two approaches. The method leverages properties of the Cumulative Absolute Error per Ray (CAER) metric with respect to the errors of pose estimates of a 2D LIDAR sensor, and utilises scan–to–map-scan matching for fine(r) pose estimations. A large number of tests, in real and simulated conditions, involving disparate environments and sensor properties, illustrate that the proposed method outperforms state-of-the-art methods of both classes of solutions in terms of pose discovery rate and execution time. The source code is available for download.

Index Terms— global localisation, 2D LIDAR, monte carlo, scan–to–map-scan matching

I. INTRODUCTION

The knowledge of a mobile robot's initial pose is a prerequisite in tasks involving its navigation, especially in contexts where an observer is used for pose tracking. However, the robot's pose is not predictable or pre-settable in all conditions. This lack of predictability necessitates ad hoc estimation without prior information. Various sensor and map modalities have been investigated in the literature; from 2D and 3D LIDAR sensors [1], [2], RGBD cameras [3], and RFID equipment [4], to keyframe-based submaps [5] and metric maps [6]. In practice the latter combined with 2D LIDAR sensors have become the de facto means of mobile robot localisation and navigation due to the sensor's high measurement precision and frequency, almost no need for preprocessing, and low cost compared to 3D LIDAR sensors.

This article addresses the problem of Passive Global Localisation of a 2D LIDAR sensor in a 2D metric map, i.e. the estimation of its location and orientation within the map, under complete locational and orientational uncertainty, without prescribing robot motion commands for further knowledge acquisition. The problem is formalised in Problem P:

Problem P. Let the unknown pose of an immobile 2D range sensor whose angular range is λ be $\boldsymbol{p}(\boldsymbol{l}, \theta)$, $\boldsymbol{l} = (x, y)$, with respect to the reference frame of map $\boldsymbol{M}$. Let the range sensor measure range scan $\mathcal{S}_R$. The objective is the estimation of $\boldsymbol{p}$ given $\mathcal{S}_R$, $\boldsymbol{M}$, and λ.

The author is with the Department of Electrical and Computer Engineering, Aristotle University of Thessaloniki, 54124 Thessaloniki, Greece
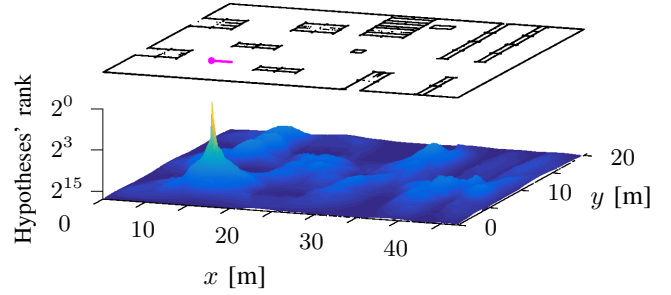`alefilot@auth.gr`

Fig. 1: Top: the map of an environment and the pose of a panoramic 2D LIDAR sensor (magenta). Given a LIDAR sensor's 2D measurement, at its core, CBGL disperses pose hypotheses within the map and ranks them ascendingly (bottom) according to the value of the Cumulative Absolute Error per Ray metric (Eq. (1)). This ranking may estimate the pose of the sensor (a) quickly due to the metric's low computational complexity, and (b) accurately due to (i) proportionality between the pose estimate error and the value of the metric for pose estimates in a neighbourhood of the sensor's pose, and (ii) lack of disproportionality outside of that neighbourhood (Fig. 2)

For the solution to Problem P this article introduces CBGL: a single-shot Monte Carlo method (a) which makes no assumptions regarding the structure or the particulars of the sensor's environment or the sensor's characteristics, (b) whose pose errors exhibit robustness to varying sensor angular range, and (c) which operates with three optionally-set and intuitive parameters, which trade accuracy for execution time. The central contributions of the article are:

- To the best of the author's knowledge the fastest Monte Carlo global localisation method that employs a 2D LIDAR that achieves higher pose discovery rates than state-of-the-art methods
- The extension and validation of the Cumulative Absolute Error per Ray metric's ability to estimate pose error hierarchies solely from real and virtual range scans, extended from scan–to–map-scan matching (sm2) during pose-tracking, where pose estimates are "few" ($\leq 2^5$) and their errors are "small", to the context of global localisation, where the set of hypotheses and their errors may be arbitrarily large
- The thorough evaluation of the proposed method against (a) established state-of-the-art localisation methods, (b) real and publicly available benchmark conditions, and (c) varying characteristics of environments and sensors, which target real conditions, that pose hindrances to global localisation methods

The rest of the article is structured as follows: Section II provides necessary definitions and the notation employed. Section III gives a brief review of solutions to problem P, and the relation of the proposed method to them. The latter's methodology is presented in section IV, its evaluation in section V, and its limitations in section VI. Section VII concludes this study.

II. DEFINITIONS AND NOTATION

Let $\mathcal{A} = \{\alpha_i : \alpha_i \in \mathbb{R}\}$, $i \in \mathtt{I} = \langle 0, 1, \ldots, n-1 \rangle$, denote a set of n elements, $\langle \cdot \rangle$ denote an ordered set, $\mathcal{A}_\uparrow$ the set $\mathcal{A}$ ordered in ascending order, the bracket notation $\mathcal{A}[\mathtt{I}] = \mathcal{A}$ denote indexing, and notation $\mathcal{A}_{k:l}$, $0 \leq k \leq l$, denote limited indexing: $\mathcal{A}_{k:l} = \{\mathcal{A}[k], \mathcal{A}[k+1], \ldots, \mathcal{A}[l]\}$.

Definition I. *Pose and pose estimate.*—The object of localisation is the estimation of the—fundamentally-unknown—3DoF pose $\boldsymbol{p}$ of a sensor or robot: $\hat{\boldsymbol{p}} = (\hat{\boldsymbol{l}}, \hat{\theta})$, where $\hat{\boldsymbol{l}} = (x, y) \in \mathbb{R}^2$ is its location on the 2D plane and $\hat{\theta} \in [-\pi, \pi)$ rad its orientation relative to the positive x axis.

Definition II. *Range scan captured from a 2D LIDAR sensor.*—A range scan $\mathcal{S}$, measured by a 2D LIDAR sensor, consisting of N_s rays over an angular range $\lambda \in (0, 2\pi]$, is an ordered map of angles to distances between objects and the sensor within its radial range $r_{\max}$: $\mathcal{S} : \Theta \to \mathbb{R}_{\geq 0}$, $\Theta = \{\theta_n \in [-\frac{\lambda}{2}, +\frac{\lambda}{2}) : \theta_n = -\frac{\lambda}{2} + \lambda \frac{n}{N_s}, n = 0, 1, \ldots, N_s-1\}$. Angles θ_n are expressed relative to the sensor's heading, in the sensor's frame of reference [7].

Definition III. *Map-scan.*—A map-scan is a virtual scan that encapsulates the same pieces of information as a scan derived from a physical sensor (Def. II). Contrary to the latter it refers to distances within a map $\boldsymbol{M}$ of an environment rather than within the environment itself; the latter is represented by $\boldsymbol{M}$ usually in Occupancy Grid or ordered Point Cloud form. A map-scan $\mathcal{S}_V^M(\hat{\boldsymbol{p}})$ is derived by locating intersections of rays emanating from a sensor's pose estimate $\hat{\boldsymbol{p}}$ and the boundaries of $\boldsymbol{M}$.

Definition IV. *The Cumulative Absolute Error per Ray metric.*—Let $\mathcal{S}_p$ and $\mathcal{S}_q$ be two range scans, equal in angular range λ and size N_s. The value of the Cumulative Absolute Error per Ray (CAER) metric $\psi \in \mathbb{R}_{\geq 0}$ between $\mathcal{S}_p$ and $\mathcal{S}_q$ is given by

$$\psi(\mathcal{S}_p, \mathcal{S}_q) \triangleq \sum_{n=0}^{N_s-1} \left| \mathcal{S}_p[n] - \mathcal{S}_q[n] \right| \tag{1}$$

Definition V. *Field densities.*—The locational and angular density, $d_{\boldsymbol{l}}, d_\alpha \in \mathbb{N}$, of a pose set $\mathcal{H} = \{\hat{\boldsymbol{p}}_i\}$ respectively denote the mean number of pose estimates dispersed on a given map $\boldsymbol{M}$ per unit area of space and per angular cycle.

Definition VI. *Admissibility of solution.*—A pose estimate $\hat{\boldsymbol{p}}(\hat{\boldsymbol{l}}, \hat{\theta}) \in \mathbb{R}^2 \times [-\pi, +\pi)$, may be deemed an admissible solution to Problem P iff $\|\boldsymbol{p} - \hat{\boldsymbol{p}}\|_2 \leq \delta$ and $\|\boldsymbol{l} - \hat{\boldsymbol{l}}\|_2 \leq \delta_{\boldsymbol{l}}$ and $|\theta - \hat{\theta}| \leq \delta_\theta$, where $\delta_{\boldsymbol{l}}, \delta_\theta, \delta \in \mathbb{R}_{>0}$: $\delta_{\boldsymbol{l}}^2 + \delta_\theta^2 = \delta^2$.

III. RELATED WORK

The literature concerning the solution to the problem of global localisation with the use of a 2D LIDAR sensor is rich. A recent and comprehensive survey on global localisation may be found in [8], while a brief overview is given below.

In broad terms global localisation approaches may be divided into two categories: (a) approaches that operate in feature space, that is, methods that extract features from measurements and the map and establish correspondences between them, and (b) approaches that directly exploit only raw measurements. In the latter category a number of methods solve the problem in an iterative Bayesian Monte Carlo fashion, i.e. by dispersing hypotheses within the map and updating the belief of the robot's pose by incorporating new measurements as it moves until estimate convergence [9]–[13]. However, the requirement of motion (a) may give rise to safety concerns (the robot may not even be visible), and (b) increases estimation time. The Monte Carlo method proposed in this article operates directly in measurement space as well but, in contrast, is not iterative, and does not require motion or more than one measurement. As a result CBGL is a single-shot global localisation approach that is able to process more hypotheses in less time, resulting in an improvement in the number of correctly estimated locations, and making it able to compete against (traditionally faster) feature-based approaches in terms of execution time.

Research on the feature-based approaches has been more extensive due to the richness, adaptability, and efficacy of methods originated in the computer vision field, and their low execution time. Relevant methods mainly perform detection of key-points in a measurement, followed by the calculation of a distinctive signature, which is then matched to similarly- and pre-computed place-signatures [1], [14]–[20]. In principle, however, unstructured environments cannot be relied upon for the existence of features due to their absence or their sparse and fortuitous distribution (although Deep Neural Network approaches have demonstrated increased performance in place recognition with the use of 3D LIDARs [21]–[23]). Structured environments, on the other hand, manifest different features depending on the particularities of the environment, where features may be present but not in a sufficiently undisturbed state by sensor noise or map-to-environment mismatch. Furthermore, feature-based methods require the tuning of parameters in a per-environment basis, which hinders the range and degree of their applicability and efficacy. In contrast CBGL (a) makes no assumptions on- and exploits no environmental structure and (b) uses three parameters, whose setting is optional and intuitive.

In sum the proposed method retains the positive qualities of the two main approaches to global localisation and avoids their pitfalls: it uses multiple hypotheses for robustness against uncertainty, assumes no motion, environmental structure, or parameter tuning in a per-environment or sensor basis, and is robust against noise. The motivation of CBGL originates from seeking to achieve a greater degree of universality, reliability, and portability across multiple

and disparate environments, by aiming to economise on the use of resources (environmental assumptions; number, type, and cost of sensors; number of measurements; time). The proposed method is most akin to the two tested methods in [24]: all three are single-shot 2D LIDAR-based Monte Carlo approaches, but CBGL computes a measure of the alignment of the measurement to the virtual scan captured from each hypothesis *before* scan–to–map-scan matching, which occurs subsequently and only for a small subset of the most-aligned virtual scans to the measurement. This, along with the low computational complexity of the alignment measure that CBGL utilises, greatly diminish its execution time. So far this alignment measure (Def. IV) has only been tested against the context of sm2 in pose tracking, i.e. for pose hypotheses in a neighbourhood of the sensor's true pose [25], [26].

IV. THE CBGL METHOD

A. Motivation

The proposed method's motivation lies in the simple but powerful fact that in general is exhibited through fig. 2: Let a pose estimate of a 2D LIDAR sensor be in a neighbourhood of its true pose within a given map (Def. I); then the value of the CAER metric (Def. IV) between the scan measured by the sensor (Def. II) and the map-scan captured from the estimate within the map (Def. III) is proportional to both the estimate's location error and orientation error. In other words comparing any two pose estimates residing in a neighbourhood of the sensor's pose in terms of a scalar value is enough to establish a pose error hierarchy between them. Moreover, this scalar locus metric is directly derivable and calculable from the assumptions of Problem P, with low computational complexity ($\mathcal{O}(N_s)$).

The relationship of proportionality between the CAER metric of a pose estimate and its location and orientation errors has been discovered and successfully exploited in the context of non-global localisation, and specifically in pose-tracking, for the production of lidar odometry [25] and the reduction of localisation's pose estimate error [26]. In this context, estimate errors are close to the origin, i.e. in contrast to the arbitrary distribution of hypotheses' errors in Monte Carlo global localisation methods.

The above motivate investigation on whether the CAER metric could prove equally beneficial in settings more uncertain than pose-tracking, that is, where the location and orientation of pose estimates extend farther away from the sensor's true location and orientation. Fig. 3 (top) shows the relations between the total errors of hypotheses and their (a) CAER values (left) and (b) resulting ranks (right), that resulted from an experimental procedure similar to that which produced fig. 2.

B. The CBGL System

By identifying the pose estimates that correspond to the bottom k CAER values, this rationale attempts to recover the identity of the pose hypotheses with the bottom k pose errors across $\mathcal{H}$. It constitutes the core of the proposed passive global localisation method, termed CBGL, and is described
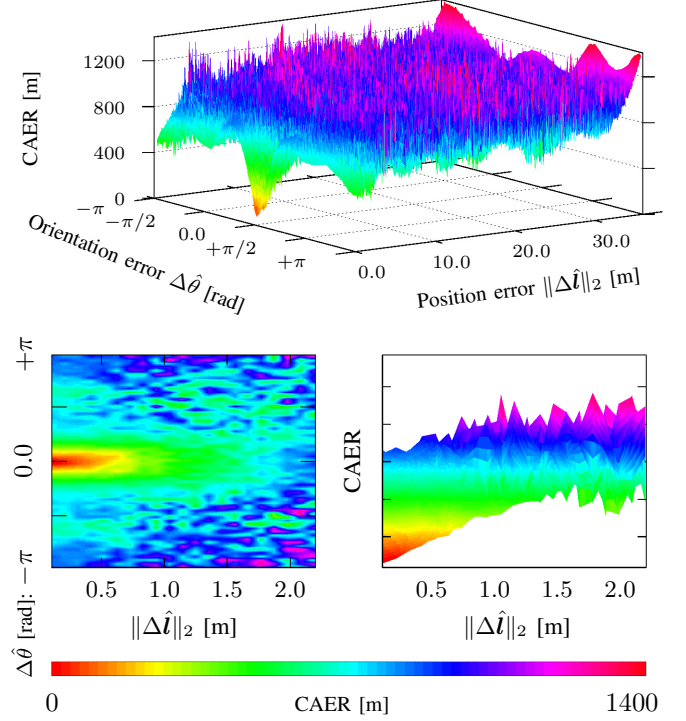

Fig. 2: Top: without loss o generality, a typical plot of the Cumulative Absolute Error per Ray metric (Eq. (1)) of 10^6 hypotheses disperesed in the map of environment WAREHOUSE (Fig. 1 and section V-B). Bottom: focused view on hypotheses with location error close to the origin
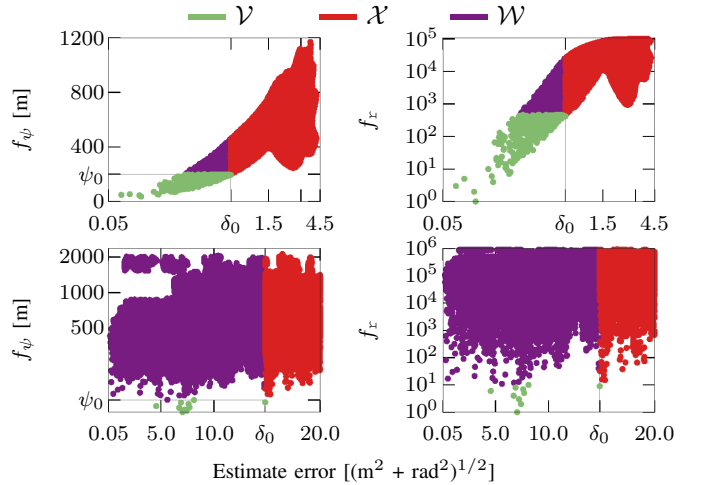

Fig. 3: The ψ-field (left) and r-field (right) of a configuration where Observation **??** may (top) and may not (bottom) be made for $\delta \leq \delta_0$. Bottom: in contrast to the top row, set $\mathcal{V}$ is empty of admissible pose estimates for $\delta < 4.5$ $(\text{m}^2 + \text{rad}^2)^{1/2}$. The effect is produced in environment WILLOWGARAGE (pose $\boldsymbol{p}_i^G$; subsection V-B) due to (a) the repetition of the immediate environment of the sensor more than once in the given map, and (b) the non-panoramic angular range of the sensor

Algorithm III `sm2`

Input: $\mathcal{S}_R$, λ, $\boldsymbol{M}$, $\hat{\boldsymbol{p}}$
Output: $\hat{\boldsymbol{p}}$ + correction that aligns $\mathcal{S}_V^M(\hat{\boldsymbol{p}})$ to $\mathcal{S}_R$
  1: $\mathcal{S}_V \leftarrow$ `scan_map`$(\boldsymbol{M}, \hat{\boldsymbol{p}}, \lambda)$
  2: $\boldsymbol{\Delta p} \leftarrow$ `scan-match`$(\mathcal{S}_R, \mathcal{S}_V)$ (e.g. `ICP` [28], `FSM` [25])

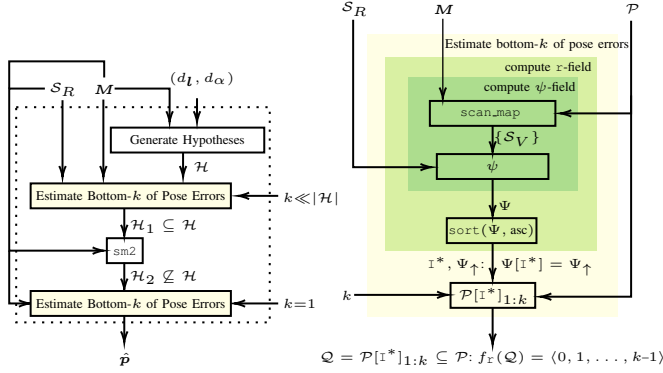 3: **return** $\hat{\boldsymbol{p}} + \boldsymbol{\Delta p}$

Fig. 4: CBGL in block diagram form. Left: Given map $\boldsymbol{M}$, CBGL first generates a set of pose hypotheses $\mathcal{H}$. Hypotheses' positions are randomly generated uniformly within the map's traversable space and orientations within $[-\pi, \pi)$ rad. Then, given a LIDAR's 2D measurement $\mathcal{S}_R$, CBGL estimates the k hypotheses with the least pose error (right; Alg. II). As a final step, it scan–to–map-scan matches $\mathcal{H}$ to $\mathcal{S}_R$ for finer estimation (`sm2`; Alg. III). CBGL's output pose estimate is that with the least CAER among the k matched estimates. Right: CBGL's core method. Given $\mathcal{S}_R$, $\boldsymbol{M}$, and pose estimates $\mathcal{P}$, it (a) computes and ranks the CAER values between $\mathcal{S}_R$ and map-scans captured from $\mathcal{P}$ within $\boldsymbol{M}$, and (b) outputs the hypotheses with the k lowest CAER values

in block diagram form in figure 4 (right) and in pseudocode in Algorithm II.

Assuming the satisfaction of Observation **??**, the challenge is choosing such k, $d_{\boldsymbol{l}}$, and d_α that, given pose estimate error requirements $\delta_{\boldsymbol{l}}$, δ_θ (Def. VI; Hyp. **??**), CBGL produces admissible pose estimates while being executed in timely manner. Given the rank field's Monte Carlo nature, optimistically, the only option for increasing the accuracy of the final pose estimate by a factor of two is doubling the densities of the `r`-field; instead of doing that—and thereby doubling the method's execution time—subsequent to the estimation of the pose estimates with the k lowest CAER values, CBGL utilises scan–to–map-scan matching [26], [27], followed by the estimation of the one pose estimate with the lowest CAER value within the group of k matched estimates. Matching allows for (a) the correction of the pose of true positive estimates by scan-matching the map-scan captured from a pose estimate against the range scan measured by the real sensor, (b) by the same token the potential divergence of spurious, false positive, pose estimates, and hence their elimination as pose estimate candidates, (c) the production of finer pose estimates without excessive increase in execution time, and (d) the decoupling of the final pose estimate's error from the field's densities. Figure 4 (left) and Algorithm I

Algorithm I `CBGL`

Input: $\mathcal{S}_R$, λ, $\boldsymbol{M}$, $(d_{\boldsymbol{l}}, d_\alpha)$, k
Output: Pose estimate of sensor measuring range scan $\mathcal{S}_R$
  1: $A \leftarrow$ `calculate_area`(`free`$(\boldsymbol{M})$)
  2: $\mathcal{H} \leftarrow \{\varnothing\}$
  3: **for** $i \leftarrow 0, 1, \ldots, d_{\boldsymbol{l}} \cdot A - 1$ **do**
  4:     $(\hat{x}, \hat{y}, \hat{\theta}) \leftarrow$ `rand()`: $(x, y) \in$ `free`$(\boldsymbol{M})$, $\hat{\theta} \in [-\pi, +\pi)$
  5:     **for** $j \leftarrow 0, 1, \ldots, d_\alpha - 1$ **do**
  6:         $\mathcal{H} \leftarrow \{\mathcal{H}, (\hat{x}, \hat{y}, \hat{\theta} + j \cdot 2\pi/d_\alpha)\}$
  7:     **end for**
  8: **end for**
  9: $\mathcal{H}_1 \leftarrow$ `bottom_k_poses`$(\mathcal{S}_R, \boldsymbol{M}, \mathcal{H}, k)$ (Alg. II)
 10: $\mathcal{H}_2 \leftarrow \{\varnothing\}$
 11: **for** $k \leftarrow 0, 1, \ldots, |\mathcal{H}_1| - 1$ **do**
 12:     $\hat{\boldsymbol{h}}' \leftarrow$ `sm2`$(\mathcal{S}_R, \lambda, \boldsymbol{M}, \mathcal{H}_1[k])$ (Alg. III or e.g. `x1` [26])
 13:     $\mathcal{H}_2 \leftarrow \{\mathcal{H}_2, \hat{\boldsymbol{h}}'\}$
 14: **end for**
 15: **return** `bottom_k_poses`$(\mathcal{S}_R, \boldsymbol{M}, \mathcal{H}_2, 1)$

present the proposed method of CBGL in block diagram and algorithmic forms respectively.

V. EXPERIMENTAL EVALUATION

This section serves the testing of the performance of state of the global localisation art methods and CBGL with regard to solving Problem P in static environments, and varying environmental conditions, sensor configurations, and map representations. With regard to CBGL its three required parameters are set to $(d_{\boldsymbol{l}}, d_\alpha, k) = (40, 2^5, 10)$ after initial tests with the dataset used in subsection V-A. The rationale of choosing appropriate $d_{\boldsymbol{l}}, d_\alpha$ is depicted in figure 5, and k is chosen as such in order to retain a high-enough true positive discovery rate without significant increase in execution time. The locational threshold $\delta_{\boldsymbol{l}} = 0.5$ m is used as a tighter inlier determinator than that of [24]; the thresold itself was determined through experimental procedure with a YDLIDAR TG30 sensor (footnote 3). References to sets $\mathcal{H}_*$ are made to fig. 4 (left) and lines 6, 9, and 13 of Algorithm I. All tests are performed with a processor of 12 threads and a clock speed of 4.00 GHz.

A. Experiments in real conditions

The first type of test is conducted using a Hokuyo UTM-30LX sensor, whose angular range is $\lambda = 3\pi/2$ rad and radial range $r_{\max} = 30.0$ m, in the Electrical and Computer Engineering Department's Laboratory of Computer Systems

Algorithm II `bottom_k_poses`

Input: $\mathcal{S}_R$, $\boldsymbol{M}$, $\mathcal{H}$, k
Output: Set of k poses of $\mathcal{H}$ with least CAER values, $\mathcal{H}_\nabla$

1: $\Psi \leftarrow \{\varnothing\}$
2: **for** $h \leftarrow 0, 1, \ldots, |\mathcal{H}| - 1$ **do**
3:     $\mathcal{S}_V^h \leftarrow$ `scan_map`$(\boldsymbol{M}, \mathcal{H}[h])$
4:     $\psi \leftarrow 0$
5:     **for** $n \leftarrow 0, 1, \ldots, |\mathcal{S}_R| - 1$ **do**
6:         $\psi \leftarrow \psi + \left| \mathcal{S}_R[n] - \mathcal{S}_V^h[n] \right|$ (Eq. (1))
7:     **end for**
8:     $\Psi \leftarrow \{\Psi, \psi\}$
9: **end for**
10: $[\Psi_\uparrow, \mathtt{I}^*] \leftarrow$ `sort`$(\Psi, \mathtt{asc})$
11: $\mathcal{H}_\nabla \leftarrow \{\varnothing\}$
12: **for** $h \leftarrow 0, 1, \ldots, k - 1$ **do**
13:     $\mathcal{H}_\nabla \leftarrow \{\mathcal{H}_\nabla, \mathcal{H}[\mathtt{I}^*[h]]\}$
14: **end for**
15: **return** $\mathcal{H}_\nabla$

	Position Err. [m]		Orientation Err. [rad]		Exec. Time [sec]	
	Mean	std	Mean	std	Mean	std
ALS	0.500	0.265	1.956	1.167	6.15	5.32
CBGL	0.041	0.045	0.011	0.019	1.61	0.06

TABLE I: Mean and standard deviation of (a) errors of ALS and CBGL with regard to position and orientation and (b) their execution times, with regard to experiments in real conditions

Architecture (CSAL), of the Aristotle University of Thessaloniki, an Occupancy Grid map of which is depicted in figure 6. The sensor was mounted on a Robotnik RB1 robot, which was teleoperated within the environment while scans were being recorded. This resulted in $N_S = 6669$ range scans, whose number of rays are downsampled by a factor of four before being inputted to CBGL and Advanced Localization System (ALS) [29]. The latter implements Free-Space Features [1] and, contrary to CBGL, it is not a single-shot method; however, it is selected for comparison against CBGL due to the fact that it is the only state of the art method which exhibits feasible execution times with respect to the collected range dataset's volume (see bottom of fig. 8b). CBGL's internal `sm2` method is chosen to be PLICP [30] due to its low execution time and the sensor's non-panoramic field of view. The top of figure 7 depicts the proportion of output pose estimates from each method whose position and orientation error is lower than outlier thresholds δ_l, δ_θ; at the bottom they are depicted exclusively for CBGL's output and its internal pose sets. Table I provides a summary of the magnitude of pose errors and execution times of the two methods.

From the experimental evidence it is clear that (a) Hypothesis **??** is observed to be true 991 times out of a thousand for an outliers' locational threshold $\delta_l = 0.5$ m when an angular threshold is δ_θ is not considered, and (b) CBGL outperforms ALS in terms of (i) number of pose estimates within all locational and angular thresholds and (ii) execution time.
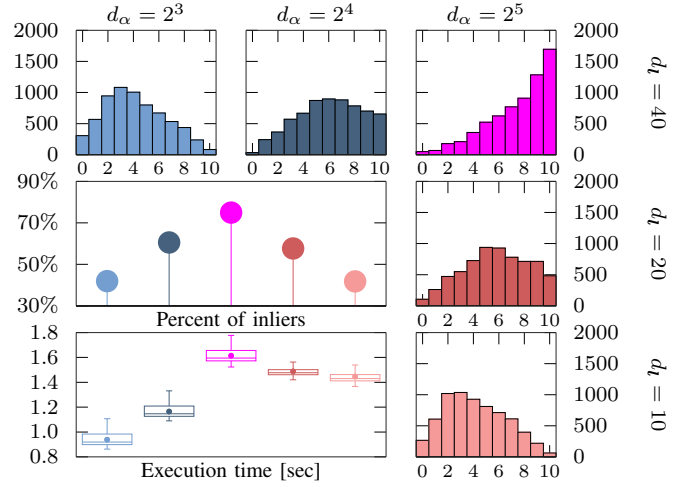

Fig. 5: Top row and right column: histograms of the number of times when exactly $n \in [0, k] = [0, 10]$ pose estimates belonging to set $\mathcal{H}_1$ exhibited pose errors lower than $\delta = (\delta_l^2 + \delta_\theta^2)^{1/2} = (0.3^2 + 0.4^2)^{1/2} = 0.5$ (m^2 + rad^2)$^{1/2}$. For densities $(d_l, d_\alpha) = (40, 2^5)$ this number is strictly increasing with n. Middle block: percent of pose estimates whose pose error is lower than δ for varying field densities. Bottom block: the distribution of corresponding execution times
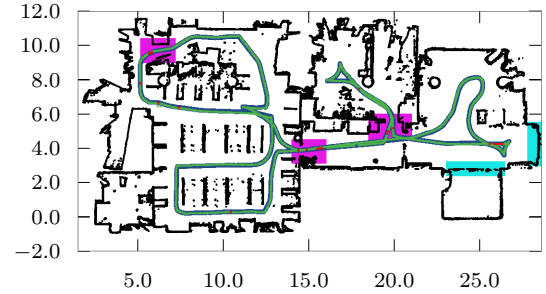

Fig. 6: The map of the real environment CSAL (black), the trajectory of the sensor (blue), and CBGL's estimated positions of the sensor (green). Sensor poses for which CBGL's output exhibits position error larger than $\delta_l = 0.5$ m are marked with red, sources of great range noise with cyan, and regions around doors with purple. A total of $N_S = 6669$ pose estimations take place, 99.1% of which result in position errors lower than δ_l. Estimation is performed for each sensor pose independently of previous estimates or measurements

B. Simulations against sources of uncertainty

The second type of test concerns the main limiting factor of global localisation methods, i.e. uncertainty—: arising e.g. from spurious measurements, repeatability of surroundings, missing or corrupted range information, or their combinations. For this reason the experimental procedure of [24] is extended here for the two methods tested therein, i.e. Passive Global Localisation-Fourier-Mellin Invariant matching with Centroids for translation (PGL-FMIC) and- Point-to-Line ICP (PGL-PLICP), and then for ALS, Monte Carlo Localisation (MCL) [9], and General Monte Carlo Localisation (GMCL) [12]. All methods are tested against the two most challenging environments, i.e. WAREHOUSE and WILLOWGARAGE, in which a panoramic range sensor is placed at 16 different poses, respectively $\boldsymbol{p}_*^W$ and $\boldsymbol{p}_*^G$, for
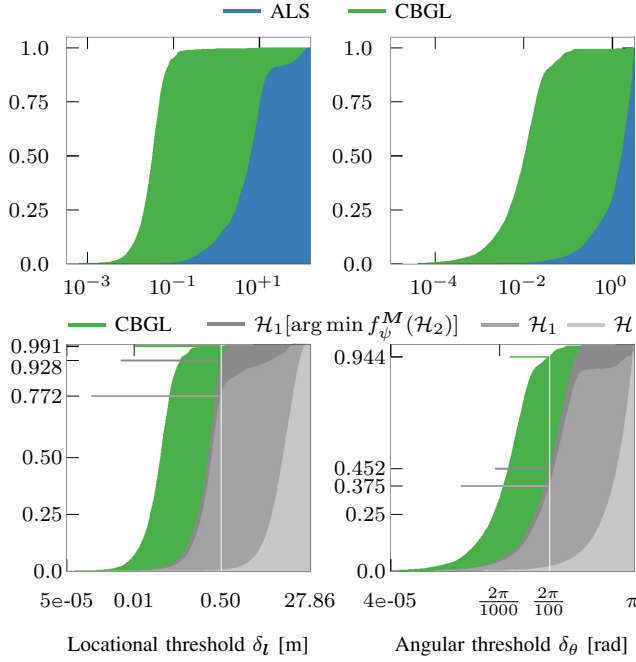
Fig. 7: Proportions of pose estimates whose position and orientation error is lower than corresponding thresholds δ_l and δ_θ. Top: ALS vs CBGL. Bottom: CBGL and internal pose estimate sets. Approximately 77% of all bottom-k pose estimates—the contents of $\mathcal{H}_1$ sets, populated via rank fields as described in sections II and IV—exhibit position errors lower than $\delta_l = 0.5$ m for $k = 10$, and so do over 99% of CBGL's final pose estimates. The improvement in position and orientation induced by scan–to–map-scan matching is captured by the difference between the output (i.e. $\mathcal{H}_2[\arg\min f_\psi^M(\mathcal{H}_2)]$) and $\mathcal{H}_1[\arg\min f_\psi^M(\mathcal{H}_2)]$
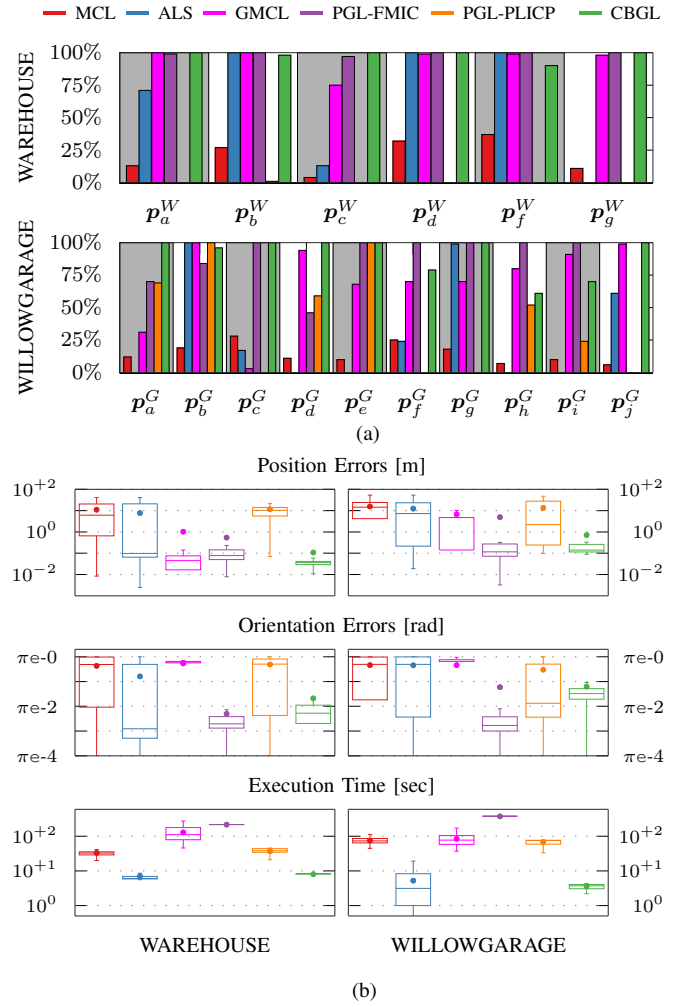

Fig. 8: (a) Percent proportions of pose outputs whose position error is lower than $\delta_l = 0.5$ m per tested environment, pose, and method. Overall CBGL (green) features the highest number of inlier poses. (b) Distribution of position errors, orientation errors, and execution times per tested environment and algorithm in seconds for $N_s = 360$ rays. CBGL's execution time is at least eighteen times lower than other Monte Carlo approaches in WILLOWGARAGE and four times lower in WAREHOUSE

$N = 100$ independent attempts at global localisation per pose. The tests are conducted with the use of a sensor whose number of rays $N_s = 360$, maximum range $r_{\max} = 10.0$ m, and noise $\sim \mathcal{N}(0, 0.05^2)$ [m,m²]. CBGL's internal sm2 method is chosen to be x1 due to the periodicity of the range signal, x1's robust pose errors compared to sm2 state of the art methods, and its greater ability in matching scans captured from higher initial displacements than ICP alternatives [26]. The latter translates to the need for smaller initial hypothesis sets: for each environment the locational density is set to 3e+04 divided by the free space area of each environment. For Monte Carlo approaches MCL and GMCL the number of initial hypotheses is also set to 3e+04.

The maximum range of the sensor is such that the geometry of environment WAREHOUSE causes (disorderly) extended lack of sampling of the sensor's surrounding environment, which limits available information and may therefore produce spurious measurements and increase r-field ambiguities between candidate estimates. In WILLOWGARAGE, on the other hand, almost all sensor placements result in complete sampling of its surroundings, but the sensor is purposefully posed in such conditions as to challenge the localisation methods' ability to perform fine distinctions between similar surroundings. Figure 8a depicts the percentage of outputs whose position error is lower than $\delta_l = 0.5$ m per tested pose, and figure 8b depicts the overall distribution of position errors, orientation errors, and execution times per tested environment and algorithm. Although the cardinality of set $\mathcal{H}$ is equal in both environments, CBGL's execution times are uneven due to x1's increased execution time when dealing with scans with missing range information. ALS is more robust against missing information than against repeated surroundings, while PGL-PLICP exhibits the inverse tendency. Notwithstanding the aforementioned sources of uncertainty, CBGL manages to exhibit the overall highest number of poses whose position error is below $\delta_l = 0.5$ m.

C. Simulations against environmental and sm2 algorithmic disparity

The third type of test aims to inquire how the performance of CBGL scales with respect to increasing environment area (and therefore to increased number of hypotheses),
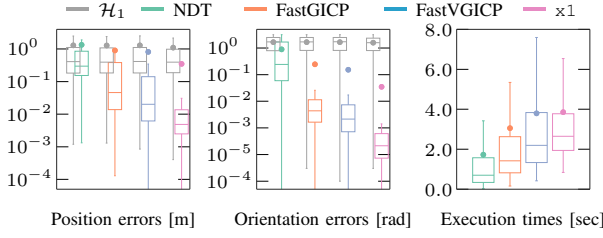
Fig. 9: Distributions of positional and orientational errors and of execution time of CBGL for varying choices of scan–to–map-scan matching methods. The errors of CBGL's internal $\mathcal{H}_1$ set are virtually unaffected by the decrease in angular range λ ($\lambda_{\text{NDT}} = \lambda_{\text{FastGICP}} = \lambda_{\text{FastVGICP}} = 3\pi/2 \neq \lambda_{\text{x1}} = 2\pi$)
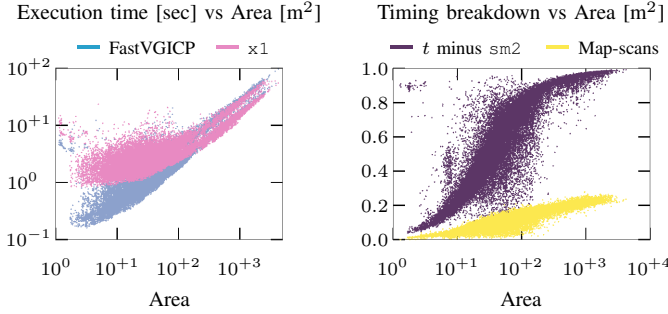

Fig. 10: Left: CBGL's execution time with respect to environment area for two choices of overlying scan–to–map-scan matching methods. In rough terms μ_t^{CBGL} [sec] $\simeq 10^{-2} \cdot area$ [m^2] for areas larger than 200 m^2. Right: Proportion of CBGL ∘ x1's total execution time spent on (a) all operations up to and except for matching, and (b) computing map-scans, with respect to area

environment diversity, sensor angular range, and choice of overlying sm2 method. CBGL is tested once in each of $N_E \simeq 4.5\text{e}+04$ environments, generated via the evaluation procedure of [26], which utilises five established and publicly available benchmark datasets provided courtesy of the Department of Computer Science, University of Freiburg [31]. Each coordinate of the Point Cloud map of each environment is corrupted by noise $\sim \mathcal{N}(0, 0.05^2)$ [m, m^2]. The angular range of the range sensor varies according to the overlying sm2 method used: for Normal Distribution Transform (NDT) [32], Fast Generalised ICP (FastGICP) [33], and Fast Voxelised Generalised ICP (FastVGICP) [34]: $\lambda = 3\pi/2$ rad; for x1: $\lambda = 2\pi$ rad. Measurement noise is $\sim \mathcal{N}(0, 0.03^2)$ [m,m^2]. As in subsection V-A the choice of field densities and k is $(d_l, d_\alpha, k) = (40, 2^5, 10)$.

Figure 9 illustrates that, with the exception of NDT, all versions of CBGL exhibit mean positional errors less than 1.0 m; its combination with x1 exhibits a mean error of approximately 0.5 m. The evidence illustrate that CBGL is robust to sensor angular range, as the distributions of errors between bottom-k ($\mathcal{H}_1$) sets are virtually indistinguishable for $k = 10$. Figure 10 shows the execution time of CBGL combined with FastVGICP and x1 as a function of environmental area, and that with x1's timing breakdown with respect to (a) CBGL's total time minus sm2 time and (b) computing map-scans, as proportions of total execution time.

VI. Characterisation & Limitations

Range scans with panoramic angular ranges induce fewer pose ambiguities in rank-fields than those with non-panoramic field of view. In the latter case this means that, given the evidence of subsections V-A and V-C where $\lambda = 3\pi/2$ rad, the choice of $k = 10$ largely inhibits the propagation of ambiguities to the output (fig. 9). However, non-panoramic sensors coupled with repeated environment structures may give rise to the conditions of figure 3 (bottom). Other sources of potential, large pose errors for CBGL are portrayed in figure 6: (a) regions coloured with cyan indicate closed glass doors, wherein high range errors result in discrepancy with map-derived virtual ranges, which is subsequently propagated to ψ-fields and hence r-fields, and (b) regions coloured purple indicate vicinities around doors, wherein higher locational density or values of k may be required to suppress pose ambiguities propagated to r-fields.

VII. Conclusions and Future Steps

This article has presented a single-shot Monte Carlo approach to the solution of the passive version of the global localisation problem with the use of a 2D LIDAR sensor, titled CBGL. CBGL allows for the fast estimation of the sensor's pose within a metric map by first dispersing hypotheses in it and then leveraging the proportionality of values of the Cumulative Absolute Error per Ray (CAER) metric to the pose errors of the hypotheses, for estimates in a neighbourhood of the sensor's pose. CBGL was evaluated in various real and simulated conditions and environments; it was found to be superior to Monte Carlo and feature-based approaches in terms of number of inlier pose estimates and execution time. Future steps will aim at the extension of the CAER metric for the use with 3D LIDAR sensors in service to a solution of the problem of their global localisation in 6DoF. The C++ ROS code of the proposed method is available at https://github.com/li9i/cbgl.

References

[1] A. Millane, H. Oleynikova, J. Nieto, R. Siegwart, and C. Cadena, "Free-Space Features: Global Localization in 2D Laser SLAM Using Distance Function Maps," in *2019 IEEE/RSJ International Conference on Intelligent Robots and Systems (IROS)*. IEEE, nov 2019, pp. 1271–1277.

[2] K. P. Cop, P. V. K. Borges, and R. Dube, "Delight: An Efficient Descriptor for Global Localisation Using LiDAR Intensities," in *2018 IEEE International Conference on Robotics and Automation (ICRA)*. IEEE, may 2018, pp. 3653–3660.

[3] Y. Guo, M. Bennamoun, F. Sohel, M. Lu, J. Wan, and N. M. Kwok, "A Comprehensive Performance Evaluation of 3D Local Feature Descriptors," *International Journal of Computer Vision*, vol. 116, no. 1, pp. 66–89, jan 2016.

[4] A. Tzitzis, A. Filotheou, A. R. Chatzistefanou, T. Yioultsis, and A. G. Dimitriou, "Real-Time Global Localization of a Mobile Robot by Exploiting RFID Technology," *IEEE Journal of Radio Frequency Identification*, pp. 1–1, 2023.

[5] S. Lowry, N. Sünderhauf, P. Newman, J. J. Leonard, D. Cox, P. Corke, and M. J. Milford, "Visual Place Recognition: A Survey," *IEEE Transactions on Robotics*, vol. 32, no. 1, pp. 1–19, feb 2016.

[6] D. M. Rosen, K. J. Doherty, A. Terán Espinoza, and J. J. Leonard, "Advances in Inference and Representation for Simultaneous Localization and Mapping," *Annual Review of Control, Robotics, and Autonomous Systems*, vol. 4, no. 1, pp. 215–242, may 2021.

[7] M. Cooper, J. Raquet, and R. Patton, "Range Information Characterization of the Hokuyo UST-20LX LIDAR Sensor," *Photonics*, 2018.

[8] H. Yin, X. Xu, S. Lu, X. Chen, R. Xiong, S. Shen, C. Stachniss, and Y. Wang, "A survey on global lidar localization: Challenges, advances and open problems," *arXiv:2302.07433*, 2023.

[9] N. Akai, L. Y. Morales, and H. Murase, "Mobile Robot Localization Considering Class of Sensor Observations," in *2018 IEEE/RSJ International Conference on Intelligent Robots and Systems (IROS)*. IEEE, oct 2018, pp. 3159–3166.

[10] J. Wang, P. Wang, and Z. Chen, "A novel qualitative motion model based probabilistic indoor global localization method," *Information Sciences*, vol. 429, pp. 284–295, mar 2018.

[11] A. Yilmaz and H. Temeltas, "Self-adaptive Monte Carlo method for indoor localization of smart AGVs using LIDAR data," *Robotics and Autonomous Systems*, vol. 122, p. 103285, dec 2019.

[12] M. A. Alshikh Khalil and I. Hatem, "Development of a new technique in ros for mobile robots localization in known-based 2d environments," *Tishreen University Journal of Research and Scientific Studies - Engineering Sciences Series*, pp. 119–137, 2021.

[13] R. Chen, H. Yin, Y. Jiao, G. Dissanayake, Y. Wang, and R. Xiong, "Deep Samplable Observation Model for Global Localization and Kidnapping," *IEEE Robotics and Automation Letters*, vol. 6, no. 2, pp. 2296–2303, apr 2021.

[14] F. Kallasi and D. L. Rizzini, "Efficient loop closure based on FALKO lidar features for online robot localization and mapping," in *2016 IEEE/RSJ International Conference on Intelligent Robots and Systems (IROS)*. IEEE, oct 2016, pp. 1206–1213.

[15] M. Usman, A. M. Khan, A. Ali, S. Yaqub, K. M. Zuhaib, J. Y. Lee, and C.-S. Han, "An Extensive Approach to Features Detection and Description for 2-D Range Data Using Active B-splines," *IEEE Robotics and Automation Letters*, vol. 4, no. 3, pp. 2934–2941, jul 2019.

[16] Z. Wang, L. Zhang, S. Zhao, and S. Zhang, "Global Localization With a Single-Line LiDAR by Dense 2D Signature and 1D Registration," *IEEE Sensors Journal*, vol. 21, no. 10, pp. 11 497–11 506, may 2021.

[17] J. Meng, L. Wan, S. Wang, L. Jiang, G. Li, L. Wu, and Y. Xie, "Efficient and Reliable LiDAR-Based Global Localization of Mobile Robots Using Multiscale/Resolution Maps," *IEEE Transactions on Instrumentation and Measurement*, vol. 70, pp. 1–15, 2021.

[18] R. W. M. Hendrikx, P. Pauwels, E. Torta, H. J. Bruyninckx, and M. J. G. van de Molengraft, "Connecting Semantic Building Information Models and Robotics: An application to 2D LiDAR-based localization," in *2021 IEEE International Conference on Robotics and Automation (ICRA)*. IEEE, may 2021, pp. 11 654–11 660.

[19] S.-Y. An and J. Kim, "Extracting Statistical Signatures of Geometry and Structure in 2D Occupancy Grid Maps for Global Localization," *IEEE Robotics and Automation Letters*, vol. 7, no. 2, pp. 4291–4298, apr 2022.

[20] K. Nielsen and G. Hendeby, "Survey on 2D Lidar Feature Extraction for Underground Mine Usage," *IEEE Transactions on Automation Science and Engineering*, vol. 20, no. 2, pp. 981–994, apr 2023.

[21] T.-X. Xu, Y.-C. Guo, Z. Li, G. Yu, Y.-K. Lai, and S.-H. Zhang, "TransLoc3D : Point Cloud based Large-scale Place Recognition using Adaptive Receptive Fields," may 2021. [Online]. Available: http://arxiv.org/abs/2105.11605

[22] P. Yin, F. Wang, A. Egorov, J. Hou, Z. Jia, and J. Han, "Fast Sequence-Matching Enhanced Viewpoint-Invariant 3-D Place Recognition," *IEEE Transactions on Industrial Electronics*, vol. 69, no. 2, pp. 2127–2135, feb 2022.

[23] J. Komorowski, "Improving Point Cloud Based Place Recognition with Ranking-based Loss and Large Batch Training," in *2022 26th International Conference on Pattern Recognition (ICPR)*. IEEE, aug 2022, pp. 3699–3705.

[24] A. Filotheou, A. Tzitzis, E. Tsardoulias, A. Dimitriou, A. Symeonidis, G. Sergiadis, and L. Petrou, "Passive Global Localisation of Mobile Robot via 2D Fourier-Mellin Invariant Matching," *Journal of Intelligent & Robotic Systems*, p. 26, 2022.

[25] A. Filotheou, G. D. Sergiadis, and A. G. Dimitriou, "FSM: Correspondenceless scan-matching of panoramic 2D range scans," in *2022 IEEE/RSJ International Conference on Intelligent Robots and Systems (IROS)*. IEEE, 2022.

[26] A. Filotheou, A. L. Symeonidis, G. D. Sergiadis, and A. G. Dimitriou, "Correspondenceless scan-to-map-scan matching of 2D panoramic range scans," *Array*, 2023.

[27] G. Vasiljević, D. Miklić, I. Draganjac, Z. Kovačić, and P. Lista, "High-accuracy vehicle localization for autonomous warehousing," *Robotics and Computer-Integrated Manufacturing*, 2016.

[28] I. Vizzo, T. Guadagnino, B. Mersch, L. Wiesmann, J. Behley, and C. Stachniss, "KISS-ICP: In Defense of Point-to-Point ICP Simple, Accurate, and Robust Registration If Done the Right Way," *IEEE Robotics and Automation Letters*, 2023.

[29] N. Akai, "Reliable monte carlo localization for mobile robots," *arXiv:2205.04769*, 2022.

[30] A. Censi, "An ICP variant using a point-to-line metric," in *2008 IEEE International Conference on Robotics and Automation*. IEEE, may 2008, pp. 19–25.

[31] "Datasets used in the experimental procedure." [Online]. Available: http://ais.informatik.uni-freiburg.de/slamevaluation/datasets.php

[32] P. Biber and W. Strasser, "The normal distributions transform: a new approach to laser scan matching," in *Proceedings 2003 IEEE/RSJ International Conference on Intelligent Robots and Systems (IROS 2003) (Cat. No.03CH37453)*, vol. 3. IEEE, 2003, pp. 2743–2748.

[33] A. Segal, D. Haehnel, and S. Thrun, "Generalized-ICP," in *Robotics: Science and Systems V*. Robotics: Science and Systems Foundation, jun 2009.

[34] K. Koide, M. Yokozuka, S. Oishi, and A. Banno, "Voxelized GICP for Fast and Accurate 3D Point Cloud Registration," in *2021 IEEE International Conference on Robotics and Automation (ICRA)*. IEEE, may 2021, pp. 11 054–11 059.